

Utilization of new computational intelligence methods to estimate daily evapotranspiration of wheat using gamma pre-processing

Nima Mohammadigolafshani^{1*}, Ali Koulaian²

(1. Master's Degree of Hydraulic Structures, Sciences and Research Branch of Islamic Azad University, Mazandaran province, P.O.BOX 4764855931, Islamic Republic of Iran;

2. Teacher of Technical and Vocational University, Bahari, Sari, Mazandaran Province, P.O.BOX 4816831167, Islamic Republic of Iran)

Abstract: Estimation of evapotranspiration (ET) is needed in water resources management, scheduling of farm irrigation, and environmental assessment. Hence, in practical hydrology, it is often crucial to reliably and constantly estimate evapotranspiration. Accordingly, three artificial intelligence (AI) techniques comprising adaptive neuro-fuzzy inference system (ANFIS), artificial neural network (ANN) and adaptive neuro-fuzzy inference-wavelet (ANFIS-Wavelet) were applied in to estimate wheat crop evapotranspiration (ET_c). A case study in a Dashtenaz region located in Mazandaran, Iran, was conducted with weather daily data, including the maximum temperature, minimum temperature, maximum relative humidity, minimum relative humidity, wind speed, and solar radiation since 2003 to 2011. The daily climatic data from Dashtenaz stations, (eight stations), were used as inputs AI models for estimating ET_0 . The assessments of the AI models were compared with the wheat crop evapotranspiration (ET_c) values measured by crop coefficient approach and standard FAO-56 Penman–Monteith equation. Similarly, determination coefficient (R^2), Nash–Sutcliffe (C_{NS}) efficiency coefficient model and root mean squared error ($RMSE$) were applied to compare the performance of models and to decide on the best one. The outcomes attained with the ANFIS-Wavelet model (with trapezoidal member function's combination with Mayer wavelet) were better than ANN and ANFIS models for ET_c estimation and confirmed the potential of this technique to provide a useful tool in ET_c modeling.

Keywords: adaptive neuro-fuzzy inference system, adaptive neuro-fuzzy inference-wavelet, evapotranspiration, neural network, wheat

Citation: Mohammadigolafshani, N., and A. Koulaian. 2018. Utilization of new computational intelligence methods to estimate daily evapotranspiration of wheat using gamma pre-processing. *Agricultural Engineering International: CIGR Journal*, 20(3): 1–12.

1 Introduction

From the physical meteorology standpoint, evapotranspiration (ET) is the collective process of evaporation from the plant and soil surfaces, and transpiration through the plant surface stomata. Consistent with Aytok (2009), ET estimation is of significance for optimizing crop production, the best management practices development to minimize groundwater and surface water degradation and the water budget determination. Evapotranspiration can either be

measured with a lysimeters or water-balance approach (as a direct method), or be estimated by applying climatic data (the indirect method). Unfortunately, lysimeters are inappropriate for observing evapotranspiration as compared to the direct climate-based measurement at weather stations. This is not only attributable to the budget and complexity, but also because the limited area of a typical weather station enclosure does not present sufficient realization from a representative surface for these measurements to be significant (Sentelhas et al., 2010). According to Pereira et al. (2002), the method selection for estimating the evapotranspiration is subjective to several factors among which the accessibility of meteorological data, as the complex methods necessitating a high number of variables, has applicability only when all necessary data are available.

Received date: 2017-06-16 Accepted date: 2017-09-24

*Corresponding author: N. Mohammadigolafshani, Master's Degree of Hydraulic Structures, Sciences and Research Branch of Islamic Azad University, Email: n.mohammadi138@yahoo.com. Tel: +989113268260.

A drawback to this approach is that the “real” reference evapotranspiration (ET_0) is unknown and can only be obtained using lysimeters or other precision measuring devices. However, several studies have been piloted using lysimeters data and have shown, on the whole, the PM as the best method for estimating ET_0 . The international scientific community has acknowledged the FAO56PM equation for its good results when compared with other equations in different regions around the world (Chiew et al., 1995; Garcia et al., 2004; Gavilán et al., 2006). When there is availability of data, Allen et al. (1998) recommended the use of the Penman-Monteith (PM) as the only standard method for defining and computing ET_0 . From the several existing ET_0 equations, presently, the FAO-56 use of the PM equations is broadly used and can be referred to as a sort of standard (Walter et al., 2000). The PM equation enjoys having two benefits over many other equations. First, it can be utilized comprehensively without any local calibrations as a result of its physical basis. Second, the equation is a well-documented equation that has been tested by applying a myriad of lysimeters (Gocic and Trajkovic, 2010). Benli et al. (2010) evaluated the six frequently utilized ET_0 estimation methods performance with multiple data requirements namely PMFAO-56, Priestley–Taylor, Radiation-FAO24, Hargreaves, Blaney–Criddle and Class A pan contrasted with lysimeters data in a semi-arid highland environment in Turkey. They concluded that the PMF-56 and Hargreaves equations were the best options to estimate ET_0 in that study area.

While the artificial intelligence (AI) techniques application (e.g., artificial neural networks, neuro-fuzzy) for ET_0 modeling has received much attention in recent years, over the previous decades, several academics conducted studies on the reliability of artificial neural network (ANN) for assessing ET_0 as a climatic variables function (Trajkovic et al., 2003; Chauhan and Shrivastava, 2009; Traore et al., 2010). Abyaneh et al. (2010) evaluated the performance of ANN and adaptive neuro-fuzzy inference system (ANFIS) Models for Garlic Crop Evapotranspiration Estimating in Hamadan. Two AI techniques, comprising ANN and ANFIS were employed to compute garlic crop water requirements in their study.

They came to the conclusion that the ANN and ANFIS techniques are appropriate for Et_c (Evapotranspiration) simulation. Kişi (2006) examined the ET_0 modeling using ANN method and ANN results were compared with the Penman and Hargreaves models. It was stated that the ANN model outperformed the empirical models. Kişi (2007) estimated ET_0 using multi-layer perceptron (MLP) method and compared test results with the Penman, Hargreaves and Turc models. It showed the superiority of the MLP to the empirical models. Trajkovic (2005) developed temperature-based RBNN models for assessing FAO-56PM ET_0 . In his study, the results matched with the Hargreaves, Thornthwaite and FAO-56PM methods and RBNN (Radial Base Neural Network) was found to be better than the empirical models. In a study of the arid and semi-arid areas of Iran, the spatially distributed maps of ET_0 were prepared using the Hargreaves equation (Sabziparvar et al., 2010). The results indicated that the expected total monthly ET_0 revealed a significant variation during the growing season (April–September) so that the region under study experienced the highest and lowest monthly ET_0 values of 250 and 80 mm in July and April, respectively. AYTEK (2009) examined the co-active neuro-fuzzy inference system (CANFIS) for daily ET_0 modeling by applying daily atmospheric parameters. They concluded that CANFIS can be proposed as an alternate ET_0 model to the current conventional methods. Tabari et al. (2012) investigated the models based on SVM (Support Vector Machine), ANFIS (Adaptive Neuro – Fuzzy Inference System), regression and climate for ET_0 modeling by applying limited climatic data in a semi-arid highland environment. The results obtained with the SVM and ANFIS models for ET_0 estimation were far better than those attained by applying the models based on regression and climate and confirmed the fitness of these techniques to provide useful tools in ET_0 modeling in semi-arid environments. Zanetti et al. (2007) estimated evapotranspiration by applying ANN and minimum climatological data. The study was conducted on the Campos dos Goytacazes County, State of Rio de Janeiro. Consistent with the results gained in this ANN testing phase, it is determined that when considering just the maximum and minimum air temperatures, it is

conceivable to estimate ET_0 in Campos dos Goytacazes.

This study aimed to compare the AI methods for simulating processes of wheat plant evapotranspiration with results derived from FAO56 PM equation under a case study in Dashtenaz in Mazandaran Province.

2 Materials and methodology

2.1 Case study

The weather data for this study were obtained from eight stations of Dashtenaz (36.37N, 53.11E; 16 m a.s.l.) located in Mazandaran Province in northern Iran, enjoying a moderate, semitropical climate with an average temperature of 25°C in summer and about 8°C in winter. Moreover, the province has a quasi-mediterranean climate, with the annual rainfall averages of 650 mm in the eastern part of Mazandaran province and more than 1300 mm in the western part. The average monthly temperature in region under study is 3°C. The mean annual rainfall is 638.2 mm (Figure 1).

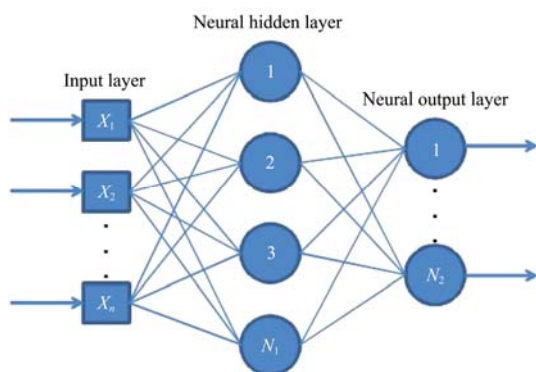


Figure 1 Architecture of neural network

The weather data were collected from the Islamic Republic of Iran Meteorological Organization (IRIMO) (www.weather.ir). The data included the mean, maximum and minimum air temperatures, relative humidity, wind speed, solar radiation and sunshine hours for the period 2003-2011. Table 1 shows some statistical data properties used in this study.

Table 1 Some statistical properties of data

Parameters	Statistical properties					
	Max	Min	Mean	Standard deviation	Covariance	Skewness
T_{min} (°C)	25.8	-2.8	11.5	6.14	0.03	0.51
T_{max} (°C)	38.2	4.8	21.5	6.87	0.03	0.49
HUM (%)	98.5	27	62.6	9.92	0.02	-0.52
R_s (hr)	13.2	0	6.6	4.18	0.11	0.13
U_2 (m s ⁻¹)	8.5	0	4.3	0.93	0.28	1.92

2.2 Climate based methods

The PMF-56 model was utilized to assess the temperature and radiation-based equations. The PMF-56 model assumes the ET_0 as that from a hypothetical crop with an assumed crop height (0.12 m) and fixed canopy resistance (70 s m⁻¹) and albedo (0.23), closely approximating the evapotranspiration from an extensive surface of green grass cover of uniform height, actively growing, and with no water shortage, which is given by (Allen et al., 1998) as follows:

$$ET_0 = \frac{0.408 \Delta (R_n - G) + \gamma [890 / (T_{mean} + 273)] U_2 (e_s - e_a)}{\Delta + \gamma (1 + 0.34 U_2)} \quad (1)$$

where, ET_0 is the reference crop evapotranspiration (mm day⁻¹); R_n is the net radiation (MJ m⁻² d⁻¹); G is the soil heat flux (MJ m⁻² d⁻¹); γ is the psychrometric constant (kPa °C⁻¹); e_s is the saturation vapor pressure (kPa); e_a is the actual vapor pressure (kPa), and Δ is the slope of the saturation vapor pressure–temperature curve (kPa °C⁻¹); T_{mean} is the daily mean air temperature (°C), and U_2 is the mean daily wind speed at 2 (m ms⁻¹). The data required for calculating ET_0 followed the method and procedure provided in Chapter 3 of FAO-56 (Allen et al., 1998).

2.3 Crop coefficient

Under standard conditions, the crop evapotranspiration denoted as ET_c , is the evapotranspiration from disease-free and well-fertilized crops, which grew in large fields, under optimum soil water conditions, and reached maximum production under the particular climatic conditions. Although the crop evapotranspiration and crop water requirement values are identical, crop water requirement concerns the amount of water that must be supplied, while crop evapotranspiration talks about the amount of water that is lost through evapotranspiration. The irrigation water requirement essentially signifies the difference between the crop water requirement and effective precipitation. The irrigation water requirement also takes in additional water for salts leaching and compensating the water application non-uniformity. The calculation of the irrigation water requirement is not included in this article. Crop evapotranspiration can be measured from climatic data through directly integrating the crop resistance, albedo and air resistance factors in the PM approach. As there is still a substantial shortage of

data for different crops, the PM method is applied to the estimation of the standard reference crop to verify its evapotranspiration rate, i.e., ET_0 . The ratios of $ET_c ET_0^{-1}$ determined in the experiment was called crop coefficients (K_c), are applied to relate ET_c to ET_0 or:

$$ET_c = K_c \cdot ET_0 \quad (2)$$

Attributable to discrepancies in the crop characteristics throughout its growing season, K_c is the given crop changes from sowing to harvest. The amounts of crop coefficients under standard conditions (ET_c) are given in Table 2.

Table 2 Crop coefficients

Month	Decade	Kc- FAO-56
December	1	0.45
	2	0.45
	3	0.45
January	1	0.45
	2	0.56
	3	0.66
February	1	0.77
	2	0.87
	3	0.99
March	1	1.09
	2	1.2
	3	1.2
April	1	1.2
	2	1.2
	3	1.2
May	1	1.2
	2	0.99
	3	0.78
June	1	0.57
	2	0.36

2.4 Gamma-test

The gamma-test (GT) measures the minimum mean square error (MSE) that can be realized when modeling the hidden data employing any continuous nonlinear models. The GT was first stated by Koncar (1997) and Agalbjorn et al. (1997), and later improved and discussed in detail by several researchers (Chuzhanova et al., 1998; De Oliveira, 1999; Tsui, 1999; Tsui et al., 2002; Durrant, 2001; Jones et al., 2002).

Simply, a concise introduction to the GT is presented here. The primary notion is quite distinctive from earlier challenges with nonlinear analysis. Assume that we have a group of data observations of the form:

$$\{(x_i, y_i), 1 \leq i \leq M\} \quad (3)$$

Where the input vectors $x_i \in R^m$ are vectors confined to some closed bounded set $C \in R^m$ and, without the loss of generality, the equivalent outputs $y_i \in R$ are scalars. The

vectors x contains predicatively useful factors influencing the output y . The only assumption made is that the underlying relationship of the system has the following form:

$$y = f(x_1, x_2, \dots, x_m) + r \quad (4)$$

where, f is a smooth function and r is a random variable that represents noise. Without loss of generality, it can be expected that the mean of the distribution of r is zero (since any constant bias can be subsumed into the unknown function f) and that the variance of the noise $\text{Var}(r)$ is bounded. The domain of a possible model is now limited to the class of smooth functions which have bounded first partial derivatives. The Gamma statistic Γ is an estimate of the model output variance that cannot be accounted by a smooth data model.

The GT is based on $N[i, k]$, which is the k_{th} ($1 \leq k \leq p$) nearest neighbors $xN[i, k]$ ($1 \leq k \leq p$) for each vector x_i ($1 \leq i \leq M$). Specifically, the GT is derived from the Delta function of the input vectors:

$$\delta_M(k) = \frac{1}{M} \sum_{i=1}^M |x_{N(i,k)} - x_i|^2 \quad 1 \leq k \leq p \quad (5)$$

where, $|\dots|$ denotes Euclidean distance, and the corresponding Gamma function of the output values:

$$\gamma_M(k) = \frac{1}{2M} \sum_{i=1}^M |y_{N(i,k)} - y_i|^2 \quad 1 \leq k \leq p \quad (6)$$

where, $y_{N(i,k)}$ is the corresponding y -value for the k_{th} nearest neighbor of x_i in Equation (5). In order to compute Γ a least squares regression line is constructed for the p points $(\delta_{(M,k)}, \gamma_{(M,k)})$

$$\gamma = A\delta + \Gamma \quad (7)$$

The graphical output of this regression line (Equation (7)) provides very useful information. First, it is significant that the vertical intercept Γ of y (or gamma) axis suggests an estimate of the best attainable MSE applying a modeling technique for unknown smooth functions of continuous variables (Evans and Jones, 2002). Second, the gradient offers an indication of the model complexity (a steeper gradient indicates a model of greater complexity).

2.5 Artificial neural network

Neural networks are made of neurons as basic units. Each neuron receives input data, and processes the input data and converts them into output forms. The input

forms may be pure data or the input results of other neurons, and the output forms may be the results of the final process or the input data of other neurons (Kim and Kim, 2008). Figure 2 is a general architecture of a feed forward neural network. This network comprises of one input layer, one or several hidden layers, and one output layer. Its learning algorithm is back-propagation (BP). In the case of the BP algorithm, first the output layer weights are updated. For each neuron of the output layer, a desired value exists. By this value and the learning rules, the weight coefficient is updated (Adineh et al., 2008). There are several features in ANN that distinguished it from the empirical models (Moghaddamnia et al., 2009). First, neural networks have flexible nonlinear function mapping capability that can approximate any continuous measurable function with arbitrarily desired accuracy, whereas most of the commonly used empirical models do not have this property. Second, being nonparametric and data-driven, neural networks impose few prior assumptions on the underlying process, from which data are generated. Also, high computation rate, learning ability through pattern presentation, prediction of unknown patterns, and flexibility affords for noisy patterns are other advantages of using ANNs (Adineh et al., 2008). In this study, several architectures and various neurons with two transfer functions embedded in the neural networks were adapted.

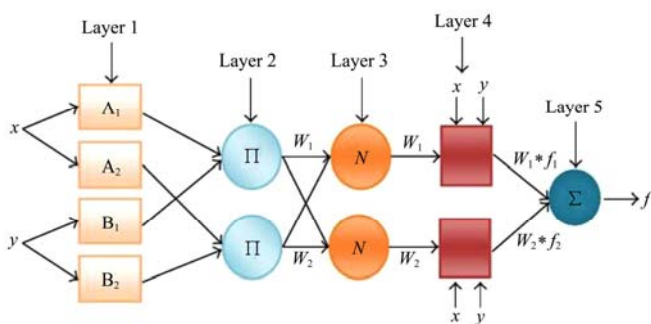


Figure 2 Architecture of adaptive neuro-fuzzy inference system

2.6 Adaptive neuro-fuzzy inference system

The ANFIS is a universal estimator and is able to approximate any real continuous function on a compact set to any degrees of accuracy (Jang et al., 1997). The basic structure of the type of fuzzy inference system could be as a model that maps input characteristics to input membership functions. Then, it relates input membership function to rules and the rules to a set of

output characteristics. Finally, it maps output characteristics to output membership functions, and the output membership function to a single output or a decision associated with the output (Jang et al., 1997). Each fuzzy system contains three main parts of fuzzifier, fuzzy database and defuzzifier. Fuzzy database includes two main parts of fuzzy rule base, and inference engine. Figure 3 represents a typical ANFIS architecture. In layer one, every node is an adaptive node with a node function such as a generalized bell membership function or a Gaussian membership function. In layer two, every node is a fixed node representing the firing strength of each rule, and is calculated by the fuzzy and connective of the ‘product’ of the incoming signals. In layer three, every node is a fixed node representing the normalized firing strength of each rule. The *i-th* node calculates the ratio of the *i-th* rule firing strength to the summation of two rules firing strengths. In layer four, every node is an adaptive node with a node function indicating the contribution of *i-th* rule toward the overall output. In layer five, the single node is a fixed node indicating the overall output as the summation of all incoming signals (Jang et al., 1997).

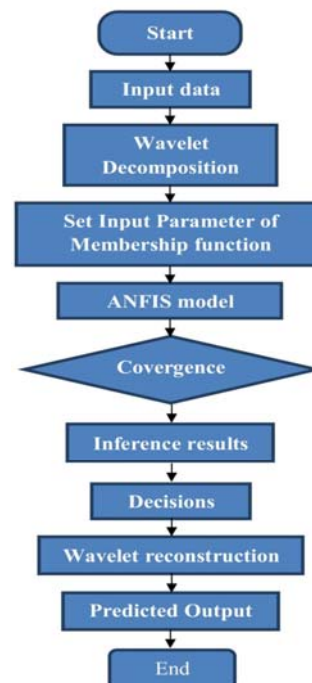


Figure 3 Structure of forecast strategy

In the present study, the Triangular, Trapezoidal, Sigmoidal, Bell, Gaussian and PI membership functions were employed. In each application, two-six numbers of MFs were tried and the best one giving the minimum of errors was selected.

2.7 Wavelet Transform

The wavelet transform of a signal is capable of providing time and frequency information simultaneously, hence providing a time–frequency representation of the signal. To accomplish this task, the data series is broken down by the transformation into its wavelets, which are a scaled and shifted version of the mother wavelet (Nason and Von Sachs, 1999). The continuous wavelet transforms (CWT) of a signal $x(t)$ is defined as follows:

$$CWT_s^\psi(s, \tau) = \frac{1}{\sqrt{|s|}} \int s(t) \psi_{s,\tau}^*(t) dt \quad (8)$$

where, s is the scale parameter; τ is the translation parameter and the ‘*’ denotes the complex conjugate. Here, the concept of frequency is replaced by that of scale, determined by the factor s . $\psi(t)$ is the transforming function, and is called the mother wavelet. The term wavelet means small wave. The smallness refers to the condition that the function is of a finite length. The wave refers to the condition that it is oscillatory. The term mother implies that the functions used in the transformation process are derived from one main function, the mother wavelet. The wavelet coefficient $CWT_x^\psi(\tau, s)$ is large when the signal $x(t)$ and the wavelet $\psi^*(t-\tau s^{-1})$ are similar; thus, the time series after the wavelet decomposition allows one to have a look at the signal frequency at different scales. The CWT calculation requires a significant amount of computation time and resources. Conversely, the discrete wavelet transforms (DWT) allows one to reduce the computation time, and is considerably simpler to implement than the CWT.

DWT scales and positions are usually based on the powers of two– the so-called dyadic scales and positions. This is achieved by modifying the wavelet representation

to:

$$\psi_{j,k}(t) = \frac{1}{\sqrt{|s_0^j|}} \psi\left(\frac{t - k\tau_0 s_0^j}{s_0^j}\right) \quad (9)$$

where, j and k are the integers and $s_0 > 1$ is a fixed dilation step. The translation factor so depends on the dilation step. The effect of discretizing the wavelet is that the time–space scale is now sampled at discrete intervals. A value of $s_0=2$ is usually chosen so that the sampling of the frequency axis corresponds to dyadic sampling. This is a very natural choice, for example, for computers, the human ear and music. A translation factor of $s_0=1$ was chosen so that there is also dyadic sampling of the time axis. High pass and low pass filters of different cutoff frequencies are used to separate the signal at different scales. The time series is decomposed into one containing its trend (the approximation) and one containing the high frequencies and the fast events (the detail). The scale is changed by above sampling and lower sampling operations. The filtering procedure is repeated every time when some portions of the signal corresponding to some frequencies are removed, obtaining the approximation and one or more details, depending on the chosen decomposition level (Noori et al., 2009).

As depicted in Figure 4, wavelet techniques are implemented in the first and last stages. The actual time-series are first decomposed into a number of wavelet coefficient signals and one approximation signal. The decomposed signals are then fed into the ANFIS at the second stage to predict the future time-series patterns for each of the signals. Finally, the predicted signals are recombined in the last stage to form the final predicted series.

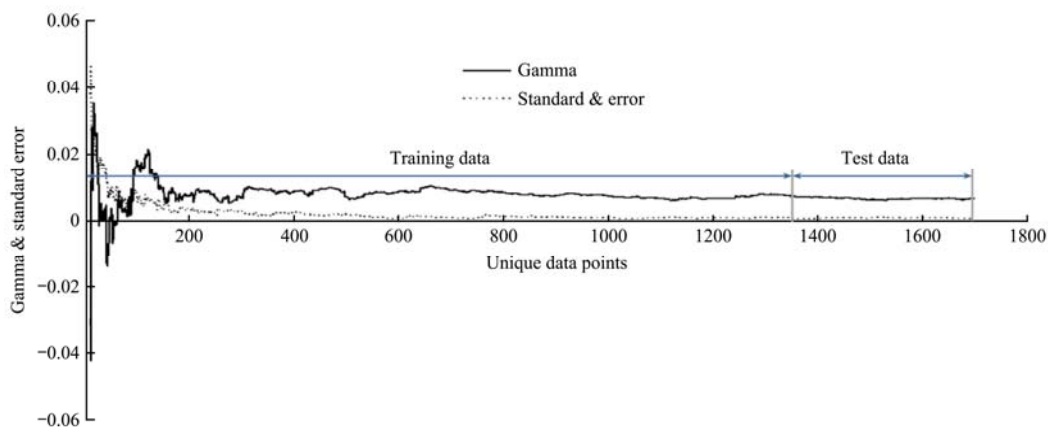


Figure 4 M-test results for the best data set

2.8 Data preprocessing

Various input combinations of data were explored in this study to assess their influence on the evapotranspiration modeling (Table 3). The best one can be specified by observing the Gamma value, indicating a measure of the best root mean square error (MSE) possible by applying any modeling methods for unseen continuous variables smooth functions. In Table 3, some very interesting variations of the best MSE are observed with different input combinations. The minimum value of Gamma was observed when all available input data sets were used, i.e. T_{\max} , T_{\min} , HUM , R_s and U_2 . The results of these tests reveal that the rate of evapotranspiration solar radiation is the most sensitive parameter, because by the removal of these data as an input, the gamma statistic will have the highest value.

Table 3 Gamma test results on different inputs

Input models combinations	Gamma	RMSE
$T_{\min}, T_{\max}, HUM, R_s, U_2$	0.006528	0.000504
$T_{\min}, T_{\max}, R_s, U_2$	0.009502	0.00078
$T_{\min}, T_{\max}, HUM, R_s$	0.010069	0.00068
T_{\min}, HUM, R_s, U_2	0.010279	0.0011
T_{\max}, HUM, R_s, U_2	0.012237	0.00098
$T_{\min}, T_{\max}, HUM, U_2$	0.021697	0.00099

The quantity of available input data to anticipate the desirable output was evaluated using the M-test. The M-test results help to determine whether there were sufficient data to provide an asymptotic Gamma estimate and subsequently a reliable model. The M-test analysis results are presented in Figure 5. As it can be witnessed from the figure, the data standard error for 1360 numbers is the lowest. This number has been selected as the training network data number. The remaining data were used to test the model and estimate the results.

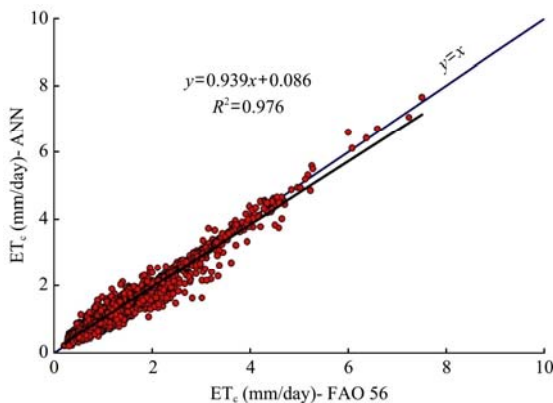


Figure 5 Scatter and time series plots of observed versus estimated wheat evapotranspiration values using ANN

2.9 Performance criteria

First, the normalization on the data is done in line with the following expression. There are two main advantages to normalize features before applying AI methods for prediction. One advantage is to avoid using attributes in greater numeric ranges that control those in smaller numeric ranges, and another advantage is to avoid numerical difficulties during the calculation. It is recommended to linearly scale each attribute to the range $(-1, 1)$ or $(0, 1)$. In the modeling process, all data values are scaled to the range between zero and 1 as follows:

$$X_n = 0.5 + 0.5 \left(\frac{X - \bar{X}}{X_{\max} - X_{\min}} \right) \quad (10)$$

where, X_n is normalization and X is actual value, but \bar{X} is data average and X_{\max} and X_{\min} are the maximum and minimum measurement values.

The performance of AI models for estimating the daily ET_c was evaluated using a wide variety of standard statistics index. A total of three different standard statistics indexes were employed including the coefficient of determination (R^2), $RMSE$, and Nash Sutcliffe coefficient (C_{NS}) (Nash and Sutcliffe, 1970; Committee, 1993).

$$R^2 = \frac{\left[\sum_{i=1}^n (ET_i - \overline{ET}_i)(ET_p - \overline{ET}_p) \right]^2}{\sum_{i=1}^n (ET_i - \overline{ET}_i)^2 \cdot \sum_{i=1}^n (ET_p - \overline{ET}_p)^2} \quad (11)$$

$$RMSE = \sqrt{\frac{\sum_{i=1}^n (ET_i - ET_p)^2}{n}} \quad (12)$$

$$C_{NS} = 1 - \frac{\sum_{i=1}^n (ET_i - ET_p)^2}{\sum_{i=1}^n (ET_i - \overline{ET}_i)^2} \quad (13)$$

where, ET_i and ET_p are the observed and predicted at time i , respectively; \overline{ET}_i and \overline{ET}_p are the observed and predicted means at time I respectively; and n is the number of data points.

3 Results and discussion

3.1 ANN results

The best ANN architecture was selected and evaluated among numerous ANN architectures. The selected ANN, or the one presenting the highest performance index and the lowest MSE, is constituted by

an input layer with 5 variables, a hidden layer (with 1 to 40 neurons) and an output layer. The activity functions of sigmoid and tan sigmoid is proposed in this study. To assess the inclusive data and the predicted results, $ET = f(T_{max}, T_{min}, HUM, R_s, U_2)$ model were used as an input for the system. In this study, the combinations of input data are separated into two types (training (80% of data) and testing (20% of data)) before entering the network. The number of hidden layers was varied, as well as the neuron numbers and activation function in each layer. A summary with the statistics performance index and MSE

obtained during the training and testing phases is given in Table 4. Table 4 presents training and testing for neural network model with both sigmoid and tan sigmoid activity function and the best architecture of network with each activity function. The performance statistics results of sigmoid activity function were 0.874, 0.958, 0.259, while the results of tan sigmoid activity function were 0.918, 0.967 and 0.246 for C_{NS} , R^2 , and $RMSE$, respectively. This result indicates the superiority of neural network with tan sigmoid activity function with 1-12-1 architecture and 12 neurons in hidden layer.

Table 4 Architectures of the tested neural networks with their respective performance index

Transfer Functions	Hidden layers neural	epochs	Network architecture	$RMSE$		R^2		C_{NS}	
				train	test	train	test	train	test
tan sigmoid	12	14	1-12-1	0.2618	0.2461	0.985	0.967	0.951	0.918
Sigmoid	15	25	1-15-1	0.2778	0.2586	0.972	0.958	0.866	0.874

Figure 6 and Figure 7 demonstrates high correlation between FAO-56 measurements and ANN results. The figure indicates that the slope and intercept of the regression equations for ANN model are significantly near to one and zero, respectively. Results obtained from ANN in estimation wheat evapotranspiration indicate high accuracy.

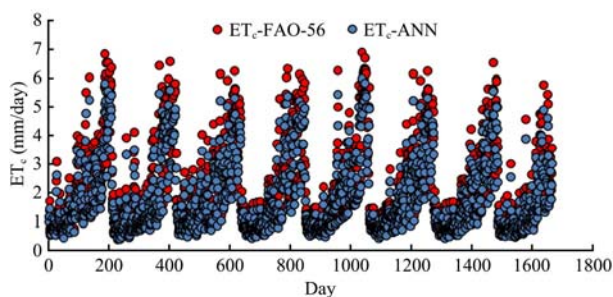


Figure 6 Scatter and time series plots of observed versus estimated values of wheat evapotranspiration from ANN for the testing data and training data

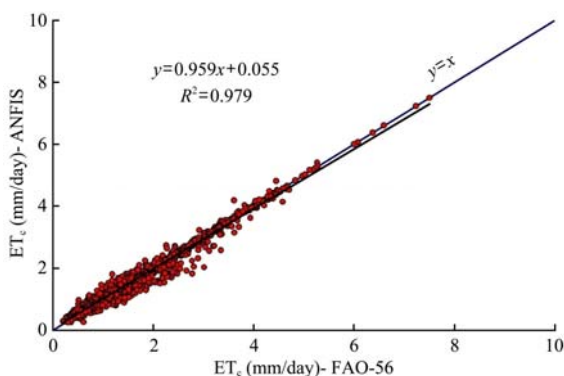


Figure 7 Scatter and time series plots of observed versus estimated values of wheat evapotranspiration from ANFIS for the testing data and training data

3.2 ANFIS results

In current study, the architecture of ANFIS with six MFs (membership functions) such as triangular, trapezoidal, bell-shaped Gaussian and Gaussian2 and PI as an input model were used. Also, the MF number was various between two to four. The ideal iterations number was obtained from trial and error procedure. The final structural design and performance statistics of the ANFIS models for the train and test phase are specified in Table 4. Two to six MFs were found to be sufficient for the ET_0 estimation using the triangular, trapezoidal, bell-shaped Gaussian and Gaussian2 and PI as an input model, respectively. Moreover, the trapezoidal function was the best MF for almost all the ANFIS models. As presented in Table 5, the trapezoidal function with inputs of the highest and lowest air temperature, solar radiation, relative humidity and wind speed had the greatest performance ($C_{NS} = 0.934$, $R^2 = 0.976$ and $RMSE = 0.039$) among the ANFIS membership functions during test. By considering each MF, ANFIS with a trapezoidal input and 4 MF number was the best model. Also, Figure 8 represents scatter plot, scatter diagram and time series of ANFIS model throughout trapezoidal membership function training and testing.

In Figure 9, although the results gained from ANFIS model for estimating ET_c are acceptable, this superiority can be demonstrated based on the regression equations slope and intercept for the ANN model (Kişi, 2007;

Keskin et al., 2009).

Table 5 Results obtained from different types of ANFIS structures and their performance evaluation

MF	OPM	Epoch	C_{NS}		R^2		$RMSE$	
			Test	Training	Test	Training	Test	Training
T_{rimf}	2	6	0.918	0.963	0.929	0.973	0.046	0.015
T_{rapmf}	4	12	0.934	0.971	0.976	0.982	0.039	0.015
G_{bellmf}	4	26	0.906	0.955	0.898	0.954	0.053	0.013
$Gauss_{mf}$	2	19	0.926	0.968	0.931	0.968	0.047	0.013
$Gauss_{2mf}$	2	15	0.811	0.946	0.809	0.941	0.088	0.028
PI_{mf}	3	24	0.856	0.941	0.889	0.923	0.057	0.028

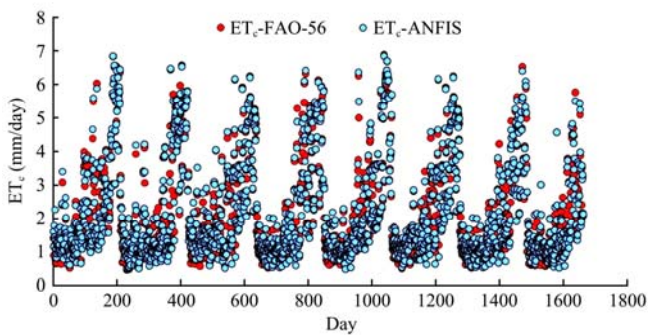


Figure 8 Scatter and time series plots of observed versus estimated values of wheat evapotranspiration from ANFIS for the testing data and training data

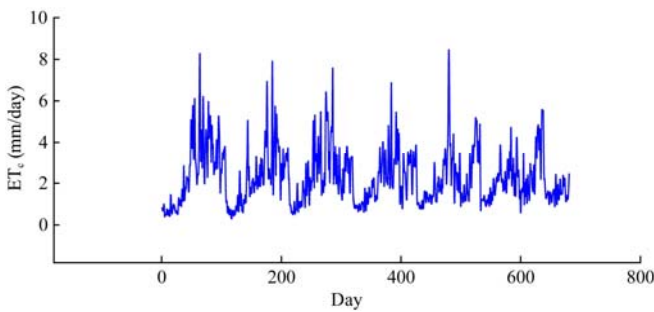
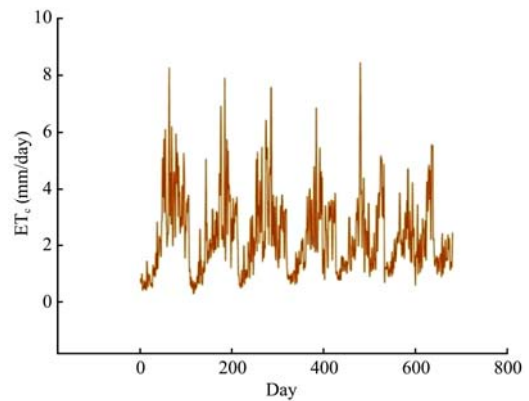


Figure 9 Time series of wheat evapotranspiration during test

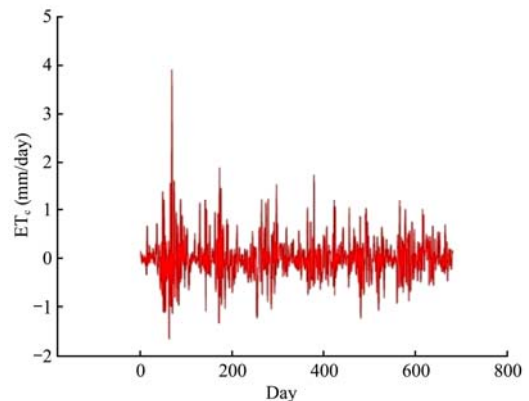
3.3 Wavelet-ANFIS results

In this section, at first the time series is separated into one comprising its trend (the approximation) and one encompassing the high frequencies and the fast events (the detail). Meyer, Symlet and Daubechies wavelets were used at this stage which is depicted in Figure 10 and Figure 11. The scale is changed by above sampling and lower sampling operations. The filtering procedure is replicated every time when some portions of the signal analogous to some frequencies are removed, obtaining the approximation and one or more details, counting on the selected decomposition level. The selection of appropriate wavelet and the decomposition levels number is highly imperative in data analysis by means of the WT. The number of decomposition levels is selected in terms

of the signal dominant frequency components. The levels are selected so that those parts of the signal that associate well with the frequencies which are needed for classification of the signal are retained in the wavelet coefficients. Then, each of the two parts is conducted separately into the ANFIS prediction model. Table 6 depicts the results of Wavelet-ANFIS. Trapezoidal member functions combination with Mayer wavelet had the best performance ($C_{NS} = 0.953$, $R^2 = 0.983$ and $RMSE = 0.0166$) during test.



(a) Part approximation



(b) Part Details

Figure 10 Time-series plot of wheat evapotranspiration during test stage using wavelet transform

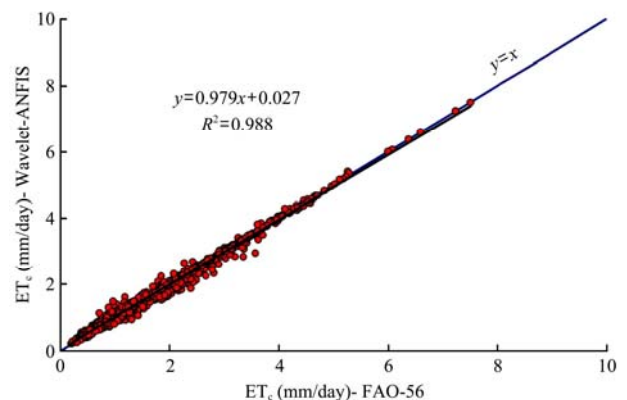


Figure 11 Scatter and time series plots of observed versus estimated values of wheat evapotranspiration from Wavelet-ANFIS for the testing data and training data

Table 6 Results obtained from different types of ANFIS-wavelet structures and their performance evaluation

Transfer function	Membership function	RMSE		R^2		C_{NS}	
		Training	Test	Training	Test	Training	Test
Meyer	Trapozal	0.008823	0.01665	0.993	0.983	0.981	0.953
Sym4	Gaussian	0.01188	0.02072	0.977	0.949	0.957	0.921
Db10	Trapozal	0.01022	0.01852	0.983	0.961	0.968	0.947

In Figure 12, although the results attained from Wavelet-ANFIS model for estimating ET_c are more acceptable than other methods, this figure also represents a fit estimated to the observed scattering and time series data and the superior model of prediction.

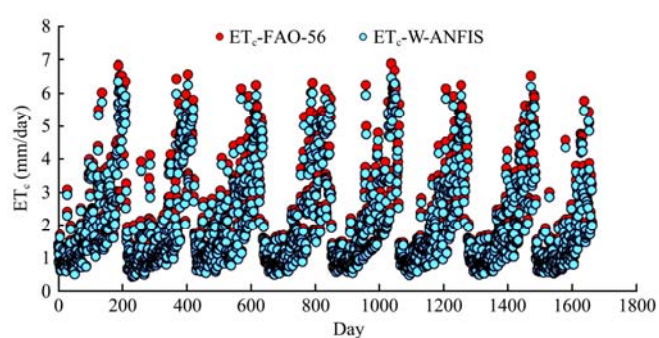


Figure 12 Scatter and time series plots of observed versus estimated values of wheat evapotranspiration from Wavelet-ANFIS for the testing data and training data

3.4 Validation performance of models

Being revealed in the results, R^2 , $RMSE$ and C_{NS} efficiency coefficient model were applied to compare the performance of models and select the best one. The outcomes of this assessment were presented in Table 7.

Table 7 Values of performance evaluation of three models

Model	C_{NS}	R^2	$RMSE$
ANN	0.935	0.967	0.2539
ANFIS	0.947	0.949	0.03
Wavelet-ANFIS	0.976	0.988	0.0124

Table 6 shows the best ANN, ANFIS, and Wavelet-ANFIS model anticipation and the data observed to estimate ET_c . As witnessed, the C_{NS} and R^2 increased from 0.935 to 0.967 and 0.976 to 0.988, respectively, and $RMSE$ has declined from 0.2539 to 0.0124. It was determined that Wavelet-ANFIS hybrid model forecasted evapotranspiration more accurately compared to ANN and ANFIS. In fact, Wavelet-ANFIS models are artificial neural networks, fuzzy logic and wavelet transform combination, making them more accurate ET_c modeling.

4 Conclusion

The applicability of ANN, ANFIS, and Wavelet-ANFIS approaches in modeling reference evapotranspiration was examined in this article. The daily climatic data from Dashtenaz stations (eight stations), Iran, were used as inputs to artificial intelligent models for assessing ET_c obtained using the standard FAO-56 Penman–Monteith equation and test results were contrasted with each other. Also, Gamma-test and M-Test were determined correspondingly for best combination of input data for measuring and testing computational models. $ET_c = f(T_{max}, T_{min}, HUM, R_s, U_2)$ models were applied as an input model of computational methods. This model includes the highest and lowest air temperature, solar radiation, relative humidity and wind speed from 2003 to 2011. Also, R^2 , $RMSE$ and C_{NS} model efficiency coefficient were utilized to compare the performance of models and decide on the best one. The results obtained with the ANFIS-Wavelet model for ET_c estimation were better than ANN and ANFIS models and confirmed the capacity of this technique to provide useful tool in ET_c modeling because random weather signals with wavelet decomposition result in reduction of noise and smoothing these signals. Results indicated that the C_{NS} and R^2 increased from 0.935 to 0.967 and from 0.976 to 0.988, respectively, and $RMSE$ has declined from 0.2539 to 0.0124 after using ANFIS-Wavelet method. This indicates the significance of the wavelet transform in various engineering fields, especially when time series prediction is non-stationary. The study presented methodology is general and if it is the accessible data with high range periods, the methodology can be employed in predicting longer time in the future.

References

- Abyaneh, H. Z., A. M. Nia, M. B. Varkeshi, S. Marofi, and O. Kisi. 2010. Performance evaluation of ANN and ANFIS models for estimating garlic crop evapotranspiration. *Journal of Irrigation and Drainage Engineering*, 137(5): 280–286.
- Adineh, V., C. Aghanajafi, G. Dehghan, and S. Jelvani. 2008. Optimization of the operational parameters in a fast axial flow CW CO₂ laser using artificial neural networks and genetic algorithms. *Optics and Laser Technology*, 40(8): 1000–1007.
- Agalbjorn, S., N. Koncar, and A. Jones. 1997. A note on the gamma

- test. *Neural Computing and Applications*, 5(3): 131–133.
- Allen, R. G., L. S. Pereira, D. Raes, and M. Smith. 1998. Crop evapotranspiration-guidelines for computing crop water requirements-FAO Irrigation and drainage paper 56. *FAO, Rome*, 300(9): D05109.
- Aytek, A. 2009. Co-active neurofuzzy inference system for evapotranspiration modeling. *Soft Computing*, 13(7): 691–700.
- Benli, B., A. Bruggeman, T. Oweis, and H. Üstün. 2010. Performance of penman-monteith FAO56 in a semiarid highland environment. *Journal of Irrigation and Drainage Engineering*, 136(11): 757–765.
- Chauhan, S., and R. Shrivastava. 2009. Performance evaluation of reference evapotranspiration estimation using climate based methods and artificial neural networks. *Water Resources Management*, 23(5): 825–837.
- Chiew, F., N. Kamaladasa, H. Malano, and T. McMahon. 1995. Penman-Monteith, FAO-24 reference crop evapotranspiration and class-A pan data in Australia. *Agricultural Water Management*, 28(1): 9–21.
- Chuzhanova, N. A., A. J. Jones, and S. Margetts. 1998. Feature selection for genetic sequence classification. *Bioinformatics*, 14(2): 139–143.
- Committee, A. T. 1993. The ASCE task committee on definition of criteria for evaluation of watershed models of the watershed management committee Irrigation and Drainage Division, Criteria for evaluation of watershed models. *Journal of Irrigation and Drainage Engineering*, 119(3): 429–442.
- De Oliveira, A. G. 1999. Synchronisation of chaos and applications to secure communications. Ph.D. diss., Imperial College of Science, Technology and Medicine, University of London.
- Durrant, P. J. 2001. WinGamma TM: a non-linear data analysis and modelling tool with applications to flood prediction. PhD thesis, Department of Computer Science, Cardiff University, Wales, UK.
- Evans, D., and A. J. Jones. 2002. A proof of the gamma test. In *Proceedings of the Royal Society of London A: Mathematical, Physical and Engineering Sciences*, The Royal Society, 2759–2799. London: 2002.
- Garcia, M., D. Raes, R. Allen, and C. Herbas. 2004. Dynamics of reference evapotranspiration in the Bolivian highlands Altiplano. *Agricultural and Forest Meteorology*, 125(1): 67–82.
- Gavilán, P., I. Lorite, S. Tornero, and J. Berengena. 2006. Regional calibration of Hargreaves equation for estimating reference ET in a semiarid environment. *Agricultural Water Management*, 81(3): 257–281.
- Gocic, M., and S. Trajkovic. 2010. Software for estimating reference evapotranspiration using limited weather data. *Computers and Electronics in Agriculture*, 71(2): 158–162.
- Jang, R., T. Sun, and E. Mizutani 1997. *Neuro-fuzzy and soft computing; a computational approach to learning and machine intelligence*. Englewood Cliffs, NJ: Prentice-Hall.
- Jones, A. J., A. Tsui, and A. De. Oliveira. 2002. Neural models of arbitrary chaotic systems: construction and the role of time delayed feedback in control and synchronization. *Complexity International*, 9: 1–9.
- Keskin, M. E., Ö. Terzi, and D. Taylan. 2009. Estimating daily pan evaporation using adaptive neural-based fuzzy inference system. *Theoretical and Applied Climatology*, 98(1-2): 79–87.
- Kim, S., and H. S. Kim. 2008. Neural networks and genetic algorithm approach for nonlinear evaporation and evapotranspiration modeling. *Journal of Hydrology*, 351(3): 299–317.
- Kişi, Ö. 2006. Evapotranspiration estimation using feed-forward neural networks. *Hydrology Research*, 37(3): 247–260.
- Kişi, Ö. 2007. Streamflow forecasting using different artificial neural network algorithms. *Journal of Hydrologic Engineering*, 12(5): 532–539.
- Koncar, N. 1997. Optimisation methodologies for direct inverse neurocontrol. Ph.D. diss., Department of Computing, Imperial College of Science, Technology and Medicine, University of London.
- Moghaddamnia, A., M. G. Gousheh, J. Piri, S. Amin, and D. Han. 2009. Evaporation estimation using artificial neural networks and adaptive neuro-fuzzy inference system techniques. *Advances in Water Resources*, 32(1): 88–97.
- Nash, J. E., and J. V. Sutcliffe. 1970. River flow forecasting through conceptual models part I—A discussion of principles. *Journal of Hydrology*, 10(3): 282–290.
- Nason, G. P., and R. V. Sachs. 1999. Wavelets in time-series analysis. *Philosophical Transactions of the Royal Society of London A: Mathematical, Physical and Engineering Sciences*, 357(1760): 2511–2526.
- Noori, R., M. A. Abdoli, A. Farokhnia, and M. Abbasi. 2009. Results uncertainty of solid waste generation forecasting by hybrid of wavelet transform-ANFIS and wavelet transform-neural network. *Expert Systems with Applications*, 36(6): 9991–9999.
- Pereira, A. R., L. R. Angelocci, and P. C. Sentelhas. 2002. *Agrometeorologia sfundamentose aplicacoes práticas, Guaíba, Agropecuária*. Lavras: Agropecuária.
- Sabziparvar, A. A., H. Tabari, A. Aeini, and M. Ghafouri. 2010. Evaluation of class a pan coefficient models for estimation of reference crop evapotranspiration in cold semi-arid and warm arid climates. *Water Resources Management*, 24(5): 909–920.
- Sentelhas, P. C., T. J. Gillespie, and E. A. Santos. 2010. Evaluation of FAO Penman–Monteith and alternative methods for estimating reference evapotranspiration with missing data in Southern Ontario, Canada. *Agricultural Water Management*, 97(5): 635–644.

- Tabari, H., O. Kisi, A. Ezani, and P. H. Talaei. 2012. SVM, ANFIS, regression and climate based models for reference evapotranspiration modeling using limited climatic data in a semi-arid highland environment. *Journal of Hydrology*, 444: 78–89.
- Trajkovic, S. 2005. Temperature-based approaches for estimating reference evapotranspiration. *Journal of Irrigation and Drainage Engineering*, 131(4): 316–323.
- Trajkovic, S., B. Todorovic, and M. Stankovic. 2003. Forecasting of reference evapotranspiration by artificial neural networks. *Journal of Irrigation and Drainage Engineering*, 129(6): 454–457.
- Traore, S., M. Wang, and T. Kerh. 2010. Artificial neural network for modeling reference evapotranspiration complex process in Sudano-Sahelian zone. *Agricultural Water Management*, 97(5): 707–714.
- Tsui, A. P., A. J. Jones, and A. G. D. Oliveira. 2002. The construction of smooth models using irregular embeddings determined by a gamma test analysis. *Neural Computing and Applications*, 10(4): 318–329.
- Tsui, A. P. M. 1999. Smooth data modelling and stimulus-response via stabilisation of neural chaos, Ph.D. diss., Department of Computing, Imperial College of Science, Technology and Medicine, University of London.
- Walter, I. A., R. G. Allen, R. Elliott, M. Jensen, D. Itenfisu, B. Mecham, T. Howell, R. Snyder, P. Brown, S. Echings, T. Spofford, M. Hattendorf, R. Cuenca, J. Wright, and D. Martin. 2000. ASCE's standardized reference evapotranspiration equation. In: *Proceedings of Fourth National Irrigation Symposium*, ASAE, Phoenix, AZ, USA, 14–16 November.
- Zanetti, S., E. Sousa, V. Oliveira, F. Almeida, and S. Bernardo. 2007. Estimating evapotranspiration using artificial neural network and minimum climatological data. *Journal of Irrigation and Drainage Engineering*, 133(2): 83–89.